

STABILITY ANALYSIS OF AUTOMOBILE DRIVER STEERING CONTROL*

R. Wade Allen

Systems Technology, Inc.
Hawthorne, California

SUMMARY

In steering an automobile the driver must basically control the direction of the car's trajectory (heading angle) and the lateral deviation of the car relative to a delineated pathway. This paper considers a previously published linear control model of driver steering behavior which is analyzed from a stability point of view. A simple approximate expression for a stability parameter, phase margin, is derived in terms of various driver and vehicle control parameters, and boundaries for stability are discussed.

A field test study is reviewed that includes the measurement of driver steering control parameters. Phase margins derived for a range of vehicle characteristics are found to be generally consistent with known adaptive properties of the human operator. The implications of these results are discussed in terms of driver adaptive behavior.

INTRODUCTION

Analysis of the closed-loop dynamic behavior of the driver/vehicle system can give some insight into driver and model behavior, and provide simplified analytical expressions for relationships between various model parameters. Here we will use a linear, two degree of freedom vehicle model. The two degrees of freedom to be considered are heading, or direction of vehicle motion, and lateral position. These two variables are under direct control of the driver. A third basic vehicle mode not considered here is roll angle. Although roll angle may influence driver behavior, it is not controlled per se by the driver. The discussion here will include a summary of previously published work (References 1 and 2).

The two degree of freedom model should be considered as an equivalent or approximation to higher degree models. Thus it subsumes such things as roll steer and weight transfer effects to a first approximation, so that the heading response of the model is an adequate approximation to a real vehicle for similar inputs.

DRIVER/VEHICLE SYSTEM MODEL

A block diagram of the driver/vehicle system model is shown in Figure 1. The vehicle equations generate side velocity (v) and yaw (heading) rate as a function of steering inputs through the G_v^s and G_δ^r transfer functions, respectively. Kinematic equations then compute vehicle heading angle and lateral lane position from side velocity and yaw rate inputs. The driver finally develops steering corrections based on perceived heading and lane position errors as processed by the behavioral transfer functions Y_v and Y_ψ .† For the closed-loop analysis reviewed here we will consider steering against disturbances applied at the steering point as shown in Figure 1.

*This work was partially funded by the Automotive Safety Affairs Office of the Ford Motor Company. However, the contents of this paper represent the views of the author and do not necessarily reflect the official views or policy of the Ford Motor Company.

†At this point a question might be raised as to why the Y_ψ block is not placed in the ψ_e pathway but rather is in the ψ_l pathway, which is the sum of the heading error and some function Y_v of lane position error y_e . This arrangement is consistent with the perceptual information most readily available to the driver, which is further described in Ref. 3.

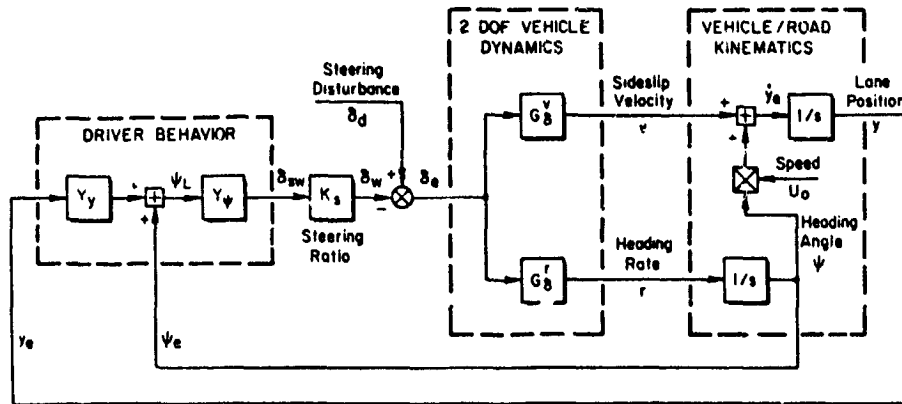


Figure 1. Driver/Vehicle Model with Two Degree of Freedom Vehicle Dynamics

This disturbance input will be used to approximate the lateral response effects of roadway disturbances on the wheels, and various forces and moments caused by roadway slope and lateral wind gusts.

The dynamics and stability of the Figure 1 system can best be analyzed by considering a steering disturbance signal (δ_d) as the input to a closed-loop system, and then analyzing the total open-loop transfer function between δ_e passing through the vehicle dynamics and driver behavior to the δ_w point. In this way we subsume the multi-path portions of the system as we progress from the single control input variable δ_e to the single control output variable δ_w .

Through simple block diagram algebra we can now derive an expression for the open-loop transfer function δ_e/δ_w as follows. First the heading angle and lane position errors can be expressed in response to δ_e inputs as

$$\psi_e = G_\delta^V \delta_e \quad ; \quad y_e = \frac{\delta_e}{s} (G_\delta^V + U_0 G_\delta^R) \quad (1)$$

Next δ_w steering response can be expressed in terms of perceived heading angle and lane position errors as

$$\delta_w = K_s \delta_{sw} = Y_\psi (\psi_e + Y_y y_e) \quad (2)$$

Combining Equations 1 and 2 we can then express the total open-loop transfer function as

$$\frac{\delta_w}{\delta_e} = Y_\psi \frac{K_s G_\delta^R}{s} \left\{ Y_y \left(\frac{G_\delta^V}{G_\delta^R} + \frac{U_0}{s} \right) + 1 \right\} \quad (3)$$

This expression can be further simplified if we now express the transfer function between heading and lane position to control input in terms of the vehicle dynamics and kinematic equations:

$$\begin{aligned} G_\delta^V &= \frac{\psi_e}{\delta_e} = \frac{G_\delta^R}{s} \\ G_\delta^R &= \frac{y_e}{\delta_e} = \frac{G_\delta^V + (U_0/s) G_\delta^R}{s} \end{aligned} \quad (4)$$

Combining Equations 3 and 4 we have

$$\frac{\delta_w}{\delta_e} = Y_\psi K_S G_\delta^\psi \left\{ Y_y \frac{G_\delta^Y}{G_\delta^\psi} + 1 \right\} \quad (5)$$

Now consider models for each of the component transfer functions in Equation 5.

Vehicle Dynamics

Two degree of freedom vehicle dynamics have previously been analyzed in some detail (Reference 1) from which the following material has been summarized. In general the transfer functions between heading angle and lane position to steering control input can be expressed by second-order equations.

$$G_\delta^\psi = \frac{N_\delta(s + 1/T_r)}{s(s^2 + 2\zeta_1\omega_1s + \omega_1^2)} \quad (6)$$

$$G_\delta^Y = \frac{Y_\delta(s^2 + 2\zeta_y\omega_y s + \omega_y^2)}{s^2(s^2 + 2\zeta_1\omega_1s + \omega_1^2)} \quad (7)$$

where T_r is the basic time constant of the vehicle's heading response and the remaining coefficients are functions of various vehicle parameters.

Using the few basic vehicle parameters described in Figure 2 and some simple assumptions we can now express Equations 6 and 7 in terms of vehicle characteristics as follows. The inverse of the heading time constant is given by

$$T_r^{-1} = \frac{2(a+b)}{mU_0a} Y_{a2} \quad (8)$$

If we now assume that the vehicle radius of gyration (k_z) is approximately equal to the geometric mean of the axle to c.g. distance:

$$k_z = \frac{I_{zz}}{m} = \sqrt{ab} \quad (9)$$

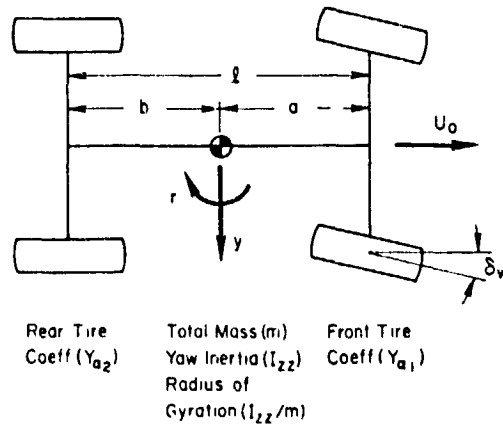


Figure 2. Vehicle Parameters for Steering Dynamics

and introduce two additional parameters, the stability factor K (sec^2/ft^2), which is related to the SAE understeer/oversteer gradient (Reference 1)

$$K \text{ (deg/sec)} = 1847(a + b)K \quad (10)$$

and the "axle load ratio"

$$v = \frac{bY_{a2}}{aY_{a1}} \quad (11)$$

we can then write approximate expressions for the remaining coefficients in Equations 6 and 7.

$$\begin{aligned} Y_{\delta} &= \frac{2}{m} Y_{a1} \quad ; \quad N_{\delta} = \frac{2a}{mk_{\delta}^2} Y_{a1} \quad ; \quad \frac{Y_{\delta}}{N_{\delta}} = \frac{k_{\delta}^2}{a} = b \\ \omega_1 &\approx T_R^{-1} \sqrt{\frac{1 + KU_{\delta}^2}{v}} \quad ; \quad \zeta_1 \approx \frac{v + 1}{2\sqrt{v(1 + KU_{\delta}^2)}} \\ 2\zeta_1\omega_1 &\approx -T_R^{-1} \left(\frac{1}{v} + 1\right) \\ \omega_y^2 &\approx T_R^{-1} \frac{U_0}{b} \quad ; \quad 2\zeta_y\omega_y \approx T_R^{-1} \end{aligned} \quad (12)$$

At best, the above expressions are good approximations for many cars. At worst the expressions should give us a qualitative feel for the lateral dynamic characteristics that are of importance to the driver.

Inspection of the above equations can give us insight into vehicle dynamic response characteristics that are important from a driver control point of view. It is obvious that the heading time constant (T_R) dominates the vehicle dynamics, and that it is a direct function of speed (Equation 8). In Equations 6 and 7 the numerator and denominator roots are an inverse function of speed (i.e., T_R^{-1}), so as the vehicle increases in speed the heading response becomes slower (lower frequency). The stability factor K can also exert further influence as a function of speed. For an oversteering car ($K < 0$) the speed sensitivity of the heading mode is even further exaggerated, while the damping decreases, causing the car to become oscillatory. For an understeering car ($K > 0$) the speed sensitivity of the heading mode denominator is reduced and the damping increases with speed.

Another factor to consider is the heading rate sensitivity to steering inputs. If we evaluate the derivative of Equation 6 at zero frequency we end up with simple expressions for steady-state heading rate and side acceleration:

$$\begin{aligned} G_{\delta}^r \quad s=0 &= U_0/l(1 + KU_{\delta}^2) \\ G_{\delta}^a \quad s=0 &= U_0^2/l(1 + KU_{\delta}^2) \end{aligned} \quad (13)$$

Here we see that steering sensitivity is a function of speed, wheelbase ($a + b = l$), and the stability factor, K . At low speeds the car follows a path whose curvature (C) is proportional to wheel deflection and inversely proportional to wheelbase (i.e., Ackermann steering):

$$C = \delta_w/l$$

Then the heading rate due to following this curved path is proportional to velocity

$$r = CU_0 = U_0 \delta_w / l$$

Therefore,

$$\frac{r}{\delta_w} = U_0 / l$$

At higher speeds the stability factor exerts additional speed effects (Equation 13), with understeering cars ($K > 0$) having less speed sensitivity and oversteering cars ($K < 0$) having increased speed sensitivity.

Driver Behavior

Given the above approximate lateral response dynamics let us now analyze the corresponding driver control dynamics for the Y_ψ and Y_y blocks of Figure 1. The Y_ψ block includes several components of driver behavior. First there is a component due to basic limitations in the driver's response properties. These limitations can be subdivided further into subcomponents: pure time delays due to central nervous system processing and neural conduction to the limbs; and interface effects due to the spring mass damping system formed by the driver's arms coupled to the steering system. Most of the neuromuscular effects are high frequency and can be approximated by a pure time delay, $e^{-\tau s}$, in the frequency range of interest for car control (Reference 4).

The second Y_ψ component is a lead or anticipation term ($T_L s + 1$) that the driver adopts to counteract vehicle response characteristics discussed above. The third component is a gain K_ψ which sets the magnitude of δ_w corrections for given heading errors (ψ_e). Combining the above components we derive a heading response function that has been developed and used in a variety of past studies (e.g., References 2 and 5):

$$Y_\psi = K_\psi (T_L s + 1) e^{-\tau s} \quad (14)$$

A pure gain feedback for lane position errors has been found satisfactory in previous research:

$$Y_y = K_y \quad (15)$$

The addition of weighted lane position error and heading angle error can actually be considered as a composite angular error as shown in Figure 1:

$$\psi_L = K_y y_e + \psi_e \quad (16)$$

It has been previously shown that this equivalent angular error can be interpreted as the angular error to a projected aim point located some distance down the road, as shown in Figure 3 (Reference 2). The aim point concept is appealing because it represents somewhat of a perceptual efficiency for the driver. Instead of separately

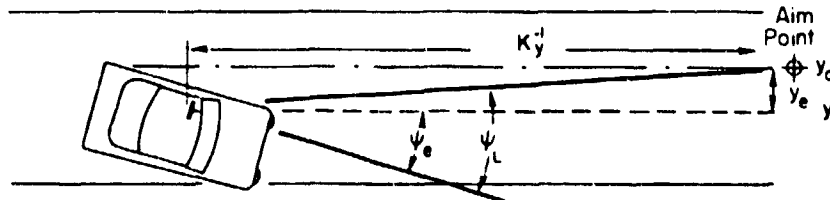


Figure 3. Aim Point Control Law. $\psi_L = \psi_e + y_e K_y$ where $\tan^{-1} y_e K_y \approx y_e K_y$

perceiving both lane position and heading errors, he need only perceive the angular error ψ_L to the aim point down the road.

One additional term will be added here that has received only scant attention in the literature (References 6 and 7). Analysis and modeling of driver response to at STI has shown the need for low-frequency characteristics or compensation that will act to reduce lane position error offsets and speed up the driver model's transient response and error reduction in tasks such as lane changes. The need for low frequency compensation can be seen by considering the effect of constant input disturbances, δ_d , to the Figure 1 block diagram. Given a constant δ_d input the driver model (i.e., Y_ψ and Y_ψ) discussed so far would have to allow constant lane position errors in order to generate a compensating wheel angle δ_w at the differential summing block. In the real world this would mean that drivers subjected to steady crosswinds or crowned roadways (i.e., inputs causing a constant force input to the vehicle) would drive with a constant lane position error.

The above offset error effect is not very reasonable, and the model can be corrected to eliminate it by adding a parallel trimming integrator, as illustrated in Figure 4, somewhere in the driver model feedforward path. The effect of the parallel integrator is to continue increasing its output in the face of steady errors, and holding its value as the errors approach zero. This will then produce steady wheel angles, δ_w , to compensate for steady disturbances, δ_d , without requiring a steady offset error.

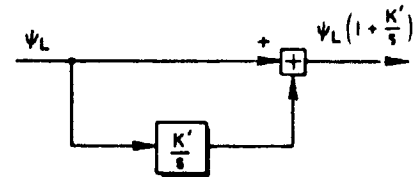


Figure 4. Parallel or "Trim Integrator for Counteracting Steady-State Error

There are two possible locations for the parallel integrator. One is in the Y_ψ block that would operate only on lane position errors. Another possibility is the Y_ψ block, where the parallel integrator would operate on the composite ψ_L signal which is a combination of lane position and heading errors. The Y_ψ location seems more reasonable for two reasons. First, the concept of perceiving a simple aim point error ψ_L would still be valid, which would not be true if the parallel integrator were applied to just the lane position errors. Second, steady-state heading errors can also develop in situations such as following curved paths, and the Y_ψ parallel integrator location would tend to compensate for these errors quicker than waiting for the heading error to accumulate into lane position errors which are operated on by the Y_ψ block.

Although we have rationalized the inner-loop (Y_ψ block) as the best location for the parallel integrator characteristic, we will analyze both possible locations (Y_ψ and Y_ψ) below in order to accumulate further evidence for the best location. Summarizing the driver response behavior for both parallel integrator locations we have:

Inner-Loop (Y_ψ) Parallel Integrator:

$$Y_\psi = \frac{s + K'}{s} K_\psi (T_L s + 1) e^{-\tau s} \quad (16)$$

$$K_y = K_y$$

Outer-Loop (Y_ψ) Parallel Integrator:

$$Y_\psi = K_\psi (T_L s + 1) e^{-\tau s} \quad (17)$$

$$Y_y = \frac{s + K'}{s} K_y$$

Driver/Vehicle Dynamics

Given the above dynamic characteristics for the vehicle and driver, let us now analyze the overall driver/vehicle system response given by Equation 5. The first term in Equation 5 (Y_ψ) is a driver characteristic, and the third is the car heading response (K_s is simply the steering ratio). The last term in Equation 5 is a combination of driver and vehicle characteristics. The interaction of these characteristics when K_y is a pure gain has been considered previously (Reference 2). Here we will consider the case where the parallel integrator is in the outer loop.

Combining Equations 5, 12, and 17 for the Y parallel integrator we end up with the following expression for the bracketed term in Equation 5

$$Y_y \frac{G_\delta^y}{G_\psi} + 1 = \frac{bK_y(s + K')[s^2 + (s/T_r) + (U_0/bT_r)]}{s^2(s + T_r^{-1})} \quad (18)$$

This can be seen to be a classical root locus problem, with one first-order zero (at K'), a second-order zero pair, two poles at the origin and a pole due to the heading time constant ($s = -1/T_r$). We can now vary the lane position gain (K_y) and plot the locus of roots for Equation 18. Root locus plots for vehicle characteristics used in past research (Reference 8) are compared in Figure 5. Here we see that with the parallel integrator in the outer loop a complex pair of low-frequency zeros occurs at reasonable values of K_y .

With the parallel integrator in the inner loop (Y_ψ , Equation 16) the result is two real zeros, one at K' and the other closed-loop zero due to the Equation 18 expression without the parallel integrator term. However, as illustrated in Figure 5, we see that for a large heading time constant the outer-loop parallel integrator always results in a complex zero with fairly low damping. This implies that the driver's low-frequency phase curve has a steep slope. However, data considered below will show that the low-frequency phase curves are never very steep and can only be fitted with two real roots as opposed to the Figure 5 complex roots.

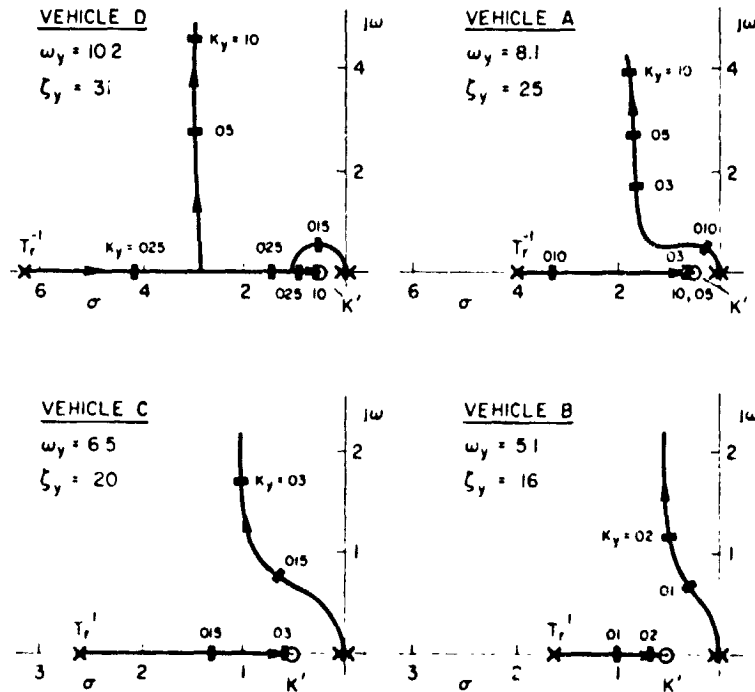


Figure 5. Root Locus for Outer-Loop Parallel Integrator (Vehicle dynamics described in Figure 6)

Phase Margin Approximation

The vehicle heading response (G_ψ) dictates the high-frequency lead compensation to be provided by the driver. Plots of G_ψ for various levels of vehicle heading time constant (T_R) studied in previous research (Reference 8) are given in Figure 6. The numerator zero and second-order denominator combine to give a net first-order-appearing transfer function combined with the kinematic integration, which gives an

VEHICLE CONFIGURATION	STEERING RATIO, K_s^{-1}	UNDERSTEER/OVERSTEER GRADIENT, K		INVERSE HEADING TIME CONSTANT, $T_F^{-1}(\text{sec}^{-1})$	INVERSE EQUIVALENT TIME CONSTANT, $T_{eq}^{-1}(\text{sec}^{-1})$	HEADING RESPONSE PARAMETERS	
		$10^4 \frac{x}{\text{sec}^2/\text{ft}^2}$	deg/g			ω_1 (rad/sec)	γ
A ———	25:1	1.1	1.9	4.0	4.9	4.5	0.79
B - - - -	17:1	1.3	2.2	1.6	2.3	2.0	0.77
C - - - -	9:1	3.3	5.7	2.6	3.9	3.5	0.61
D - - - -	11:1	3.4	5.8	6.4	7.2	6.9	0.65

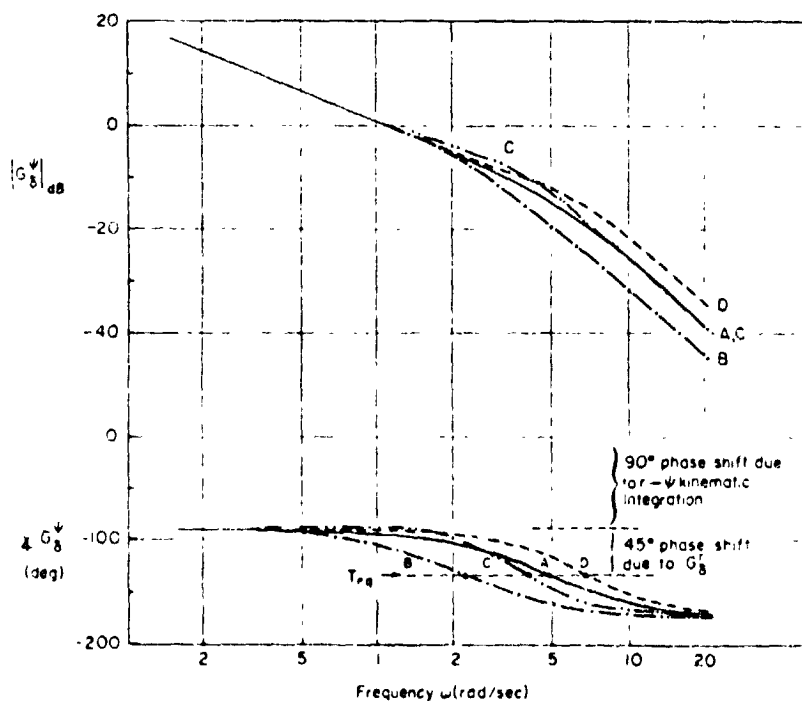


Figure 6. Test Vehicle Heading Response Transfer Functions

additional free s in the denominator. Inspection of the Figure 6 phase curves shows that the heading response dynamics can be described by an equivalent time constant, T_{eq} , which should dictate required driver lead compensation (i.e., $T_L = T_{eq}$).

Given the above components the composite driver/vehicle open-loop transfer function can be written as follows:

$$\frac{\delta_w}{\delta_e} = \underbrace{\frac{K_s K_\psi (s + K')(T_L s + 1)}{s}}_{\text{Driver Operation on Aim Point Error}} e^{-\tau s} \times \underbrace{\frac{N_\delta (s + T_r^{-1})}{s(s^2 + 2\zeta_1 \omega_1 s + \omega_f^2)}}_{\text{Vehicle Heading Response}} \times \underbrace{\frac{[s + (T_r')^{-1}](s + \alpha)}{s(s + T_r^{-1})}}_{\text{Driver/Vehicle Interaction Due to Outer-Loop Closure}} \quad (19)$$

where $\alpha = K_y U_0$. This equation can be rearranged according to frequency characteristics:

$$\frac{\delta_w}{\delta_e} = \underbrace{\frac{(s + K')(s + \alpha)}{s^2}}_{\text{① Low-Frequency Compensation}} \times \underbrace{\frac{K_y K_s N_\delta}{s}}_{\text{② Low Frequency K/s Slope}} \times \underbrace{\frac{(s + T_r^{-1})}{(s^2 + 2\zeta_1 \omega_1 s + \omega_f^2)}}_{\text{③ Mid-High Frequency Vehicle Heading Response}} \times \underbrace{\frac{s + (T_r')^{-1}}{s + T_r^{-1}}}_{\text{④ Mid-High Frequency Interaction Due to Driver/Vehicle Interaction}} \times \underbrace{(T_L s + 1)}_{\text{⑤ Driver Lead Compensation for Vehicle Heading Response Lag}} \times \underbrace{e^{-\tau s}}_{\text{⑥ Driver High-Frequency Delay Limitation}} \quad (20)$$

Now assume the driver adjusts T_L to compensate for combined phase lag characteristics of Terms ③ and ④. The 45 deg phase lag point of ③ is somewhat higher than T_r^{-1} and defines T_{eq} . Additional phase lead is derived from ④ so that the T_L^{-1} frequency break may be somewhat higher than T_r^{-1} or ω_f .

Given the complete transfer function expression above, it is now useful to consider an extended crossover model approximation. Assume that Expressions ③ and ④ combine into an equivalent first-order lag which is cancelled by the driver's lead term:

$$\frac{s + T_r^{-1}}{s^2 + 2\zeta_1 \omega_1 s + \omega_f^2} \times \frac{s + (T_r')^{-1}}{s + T_r^{-1}} \times (T_L s + 1) \approx \frac{T_r^{-1}}{\omega_f^2} \quad (21)$$

Then the driver/vehicle equivalent open-loop transfer function reduces to

$$\frac{\delta_w}{\delta_e} = \frac{(s + K')(s + \alpha)}{s^2} \times \frac{\omega_c}{s} \times e^{-\tau s} \quad (22)$$

where

$$\omega_c = \frac{K_y K_s N_\delta T_r^{-1}}{\omega_f^2} = \frac{K_y K_s U_0}{t}$$

for a neutral steering car and τ_e is an effective system time delay that accounts for the driver's time delay (τ) and residual phase lags (or lead) left over from the approximations in Equation 21.

Now we can analyze Equation 22 to determine the stability limit for the driver K_y gain. For stability the unity magnitude of Equation 22 must occur below the 180 deg phase lag point. At high frequencies ($\omega \gg K'$ and a) the unity gain point is given by ω_c (i.e., the unity gain crossover frequency) and the Equation 22 phase is given by

$$\frac{\delta_w}{\delta_e} = -\frac{\pi}{2} - \tan^{-1} \frac{K'}{\omega_c} - \tan^{-1} \frac{a}{\omega_c} - \tau_e \omega \quad (23)$$

Phase margin is defined at the gain crossover frequency ω_c , which occurs at relatively high frequency, so that

$$\tan^{-1} \frac{K'}{\omega_c} \approx \frac{K'}{\omega_c} \quad ; \quad \tan^{-1} \frac{a}{\omega_c} \approx \frac{a}{\omega_c}$$

Thus the phase margin, or amount of extra phase shift allowable before instability is reached, is given by

$$\phi_M = 2\pi - \frac{\delta_w}{\delta_e} \omega_c = \frac{\pi}{2} - \frac{K' + K_y U_0}{\omega_c} - \tau_e \omega_c \quad (24)$$

The second term on the right side of Equation 24 is the phase lag due to the driver's low frequency behavior in controlling lane deviations. The third term is the phase lag due to the driver's basic time delay limitation, which defines the limiting bandwidth he/she can achieve. Note that the outer-loop operations (K' and K_y) add phase lag and further limit the achievable bandwidth, so that the driver must trade off inner- and outer-loop gains (i.e., K_y and K' , K_y) in order to optimize performance.

Model Validation

A field study using an instrumented car on a closed test course has been previously reported on in Reference 8. The dynamics of the test vehicle could be easily modified, and the conditions given in Figure 6 were included in a test program involving 8 males and 8 females, ages 25-40, with an average of 13 years driving experience. Describing functions were obtained for each set of vehicle dynamics using a measurement technique reported previously (Reference 2).

Averaged driver describing function data for each set of vehicle dynamics are shown in Figure 7, along with curve fits according to the model of Equations 19 and 20. Some data reinterpretation over that reported in Reference 8 was necessary in order to obtain detailed model fits. Although each vehicle data set was fit individually, some constraints were observed across vehicles in order to obtain parameter values that changed in an orderly manner with vehicle heading time constant.

Model parameters are plotted as a function of inverse equivalent vehicle time constant (i.e., the basic bandwidth of vehicle heading or yawing response) in Figure 8. In general, the trends shown in Figure 8 are consistent with the known behavior of the human operator (Reference 4), to wit:

- Lead generation (T_L) increases with increasing system lag (T_{eq}), although the cancellation is not complete.
- Operator time delay (τ) increases with lead generation (T_L).
- Open-loop gain ($K_y K_c$) decreases with increasing system lag to maintain stability.

In this case of multiple-loop dynamics we also note that the outer-loop gain (K_y) decreases with increasing vehicle lag, which according to Equation 24 also tends to maintain stability.

ORIGINAL PAGE IS
OF POOR QUALITY

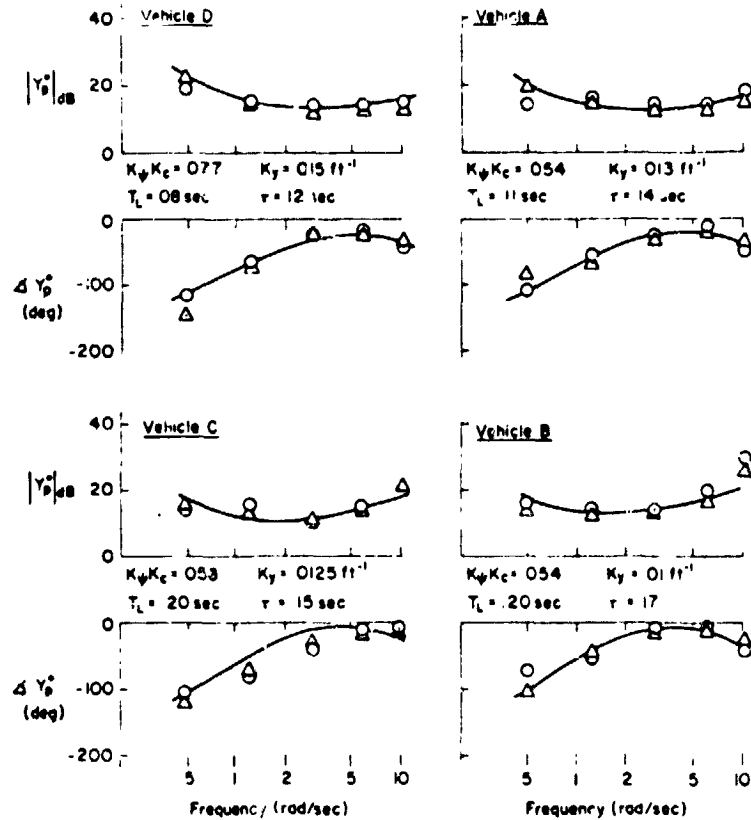


Figure 7. Field Test Driver/Vehicle Describing Functions and Model Fits (○ Male, △ Female)

The equivalent crossover model parameters plotted in Figure 9 give further insight into the driver's adaptation to different vehicle dynamics. Here we see that the phase lag component due to the driver's lane control behavior $[(K' + K_y U_0)/\omega_c]$ is maintained relatively constant. This is accomplished by reducing K_y as ω_c is reduced in response to increased system time delay (τ_e) which in turn results from increased vehicle lags.

CONCLUDING REMARKS

The approximate driver/vehicle steering dynamics analysis developed herein provides insight into the driver's adaptive behavior. The driver offsets increased vehicle lags with anticipation or lead behavior, but in doing so incurs additional time delay penalty. The driver then compensates for the phase lag due to extra time delay by reducing his/her gain.

The effect of the driver's inherent time delay penalty on stability is analyzed with a phase margin approximation. This approximation shows that both crossover frequency and outer-loop gain affect steering stability. Thus, the driver's behavior in controlling lane position results in a phase lag penalty which influences the directional stability of the driver/vehicle system.

The analysis in this paper relates to directional control stability independent of the path the driver is commanded to follow. Path commands due to roadway curvature evoke additional driver behavior which has been considered previously in References 3 and 5.

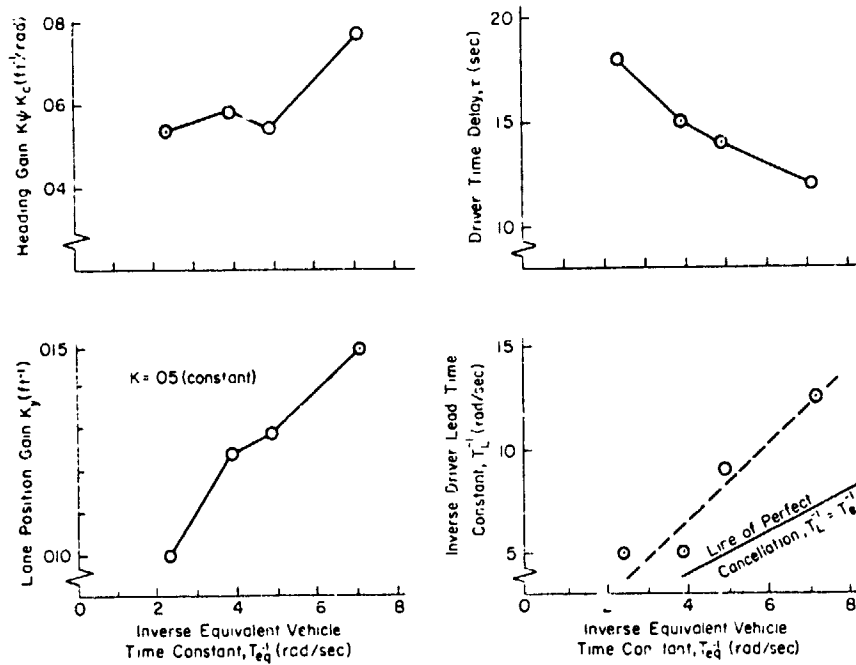


Figure 8. Effects of Vehicle Dynamics on Driver Model Parameters

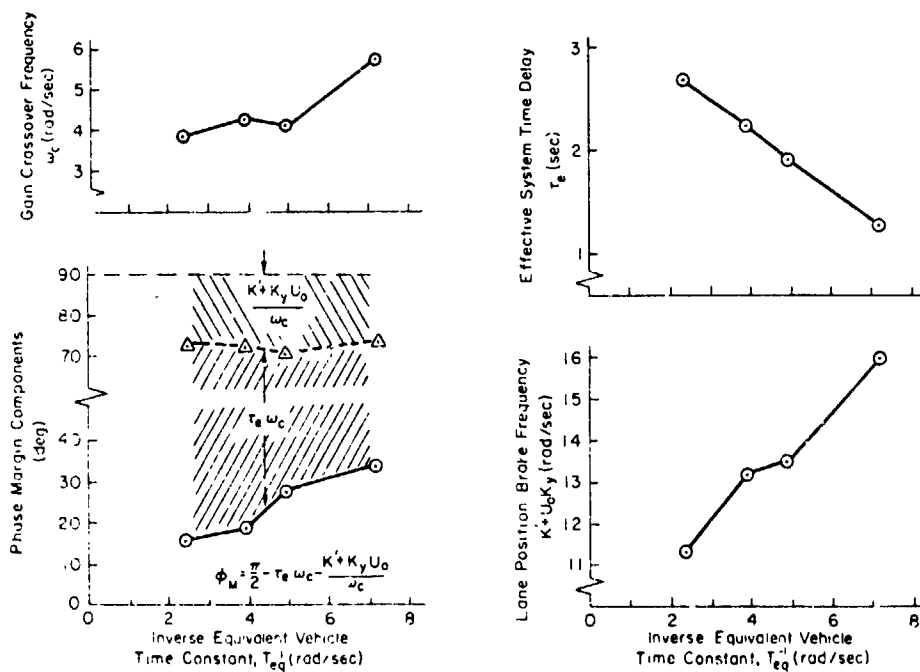


Figure 9. Effects of Vehicle Dynamics on Driver Crossover Model Parameters

REFERENCES

1. McRuer, D. T.: Simplified Automobile Steering Dynamics for Driver Control. Presented at SAE Aerospace Control and Guidance Systems Committee Meeting No. 35, Palo Alto, CA, 19-21 Mar. 1975 (Systems Technology, Inc., P-165).
2. McRuer, D. T.; Weir, D. H.; Jex, H. R.; Magdaleno, R. E.; and Allen, R. W.: Measurement of Driver/Vehicle Multiloop Properties with a Single Disturbance Input. In IEEE Transactions on Systems, Man and Cybernetics, Vol. SMC-5, No. 5, Sept. 1975, pp. 496-497.
3. Allen, R. W.; and McRuer, D. T.: The Effect of Adverse Visibility on Driver Steering Performance in an Automobile Simulator. In SAE Transactions, 1977, pp. 1081-1092.
4. McRuer, D. T.; and Krendel, E. S.: Mathematical Models of Human Pilot Behavior. AGARD-AG-188, Jan. 1974.
5. Allen, R. W.; and McRuer, D. T.: Driver Steering Dynamics Measured in a Car Simulator Under a Range of Visibility and Roadmarking Conditions. In Proceedings of the 13th Annual Conference on Manual Control. NASA CR-158107, 1977, pp. 180-196.
6. Deip, P.; Crossman, E. R. F. W.; and Szostak, H.: Estimation of Automobile Driver Describing Functions from Highway Tests Using the Double Steering Wheel. In Proceedings of the 7th Annual Conference on Manual Control. NASA SP-281, 1971, pp. 223-236.
7. Crossman, E. R. F. W.; and Szostak, H. T.: Man-machine Models for Car Steering. In Proceedings of the 4th Annual Conference on Manual Control. NASA SP-192, 1969, pp. 171-195.
8. McRuer, D.; and Klein, R.: Effects of Automobile Steering Characteristics on Driver/Vehicle Performance for Regulation Tasks. Paper 760778, presented at SAE Automobile Engineering Meeting, Detroit, 18-22 Oct. 1976.